


AUTHOR QUERY FORM

	<p>Journal: APPLES</p> <p>Article Number: 100014</p>	<p>Please e-mail your responses and any corrections to:</p> <p>E-mail: correctionsaptara@elsevier.com</p>
---	--	---

Dear Author,

Please check your proof carefully and mark all corrections at the appropriate place in the proof (e.g., by using on-screen annotation in the PDF file) or compile them in a separate list. Note: if you opt to annotate the file with software other than Adobe Reader then please also highlight the appropriate place in the PDF file. To ensure fast publication of your paper please return your corrections within 48 hours.

Your article is registered as a regular item and is being processed for inclusion in a regular issue of the journal. If this is NOT correct and your article belongs to a Special Issue/Collection please contact a.sampath@elsevier.com immediately prior to returning your corrections.

For correction or revision of any artwork, please consult <http://www.elsevier.com/artworkinstructions>

Any queries or remarks that have arisen during the processing of your manuscript are listed below and highlighted by flags in the proof. Click on the 'Q' link to go to the location in the proof.

Location in article	Query / Remark: click on the Q link to go Please insert your reply or correction at the corresponding line in the proof
Q1	AU: The author names have been tagged as given names and surnames (surnames are highlighted in teal color). Please confirm if they have been identified correctly.
Q2	AU: Keywords have been extracted from the transmittal form, please validate.
Q3	AU: This section comprises references that occur in the reference list but not in the body of the text. Please position each reference in the text or, alternatively, delete it.
Q4	AU: Please provide volume number for Ref. "Passian and Thundat, 2011".
Q5	<p>AU: Please check and validate article title for Ref. "Taylor, 1968", correct if necessary.</p> <div data-bbox="561 1451 1182 1556" style="border: 1px solid black; padding: 5px; margin: 10px auto; width: fit-content;"> <p style="color: red; text-align: center;">Please check this box or indicate your approval if you have no corrections to make to the PDF file</p> </div>

Thank you for your assistance.



ELSEVIER

Contents lists available at ScienceDirect

Applications in Engineering Science

journal homepage: www.elsevier.com/locate/apples

Experimental characterization of pull-in parameters for an electrostatically actuated cantilever

A. Sorrentino, G. Bianchi*, D. Castagnetti, E. Radi

Dipartimento di Scienze e Metodi dell'Ingegneria, Università di Modena and Reggio Emilia, Via G. Amendola 2, 42122 Reggio Emilia, Italy

ARTICLE INFO

Keywords:

Pull-In instability
MEMS
Cantilever actuators
Experimental validation

ABSTRACT

MEMS-NEMS applications extensively use micro-nano cantilever structures as actuation system, thanks to their intrinsically simple end efficient configuration. Under the action of an electrostatic actuation voltage the cantilever deflects, until it reaches the maximum value of the electrostatic actuation voltage, namely the pull-in voltage. This limits its operating point and is a critical issue for the switching of the actuator. The present work aims to experimentally measure the variation of the pull-in voltage and the tip deflection for different geometrical parameters of an electrostatically actuated cantilever. First, by relying on a nonlinear differential model from the literature, we designed and built a macro-scale cantilever switch, which can be simply adapted to different configurations. Second, we experimentally investigated the effect of the free length of the suspended electrode, and of the gap from the ground, on the pull-in response. The experimental results always showed a close agreement with the analytical predictions, with a maximum relative error lower than 10% for the pull-in voltage, and a relative difference lower than 18% for the pull-in deflection.

1. Introduction

This work experimentally investigates the pull-in instability of an electrostatically actuated cantilever beam, which reproduces the typical behavior of the micromechanical switching blocks in MEMS and NEMS applications. The interesting properties of the MEMS devices typically arise from the behavior of the active parts, which, in most cases, are in the forms of cantilevers (Ke et al., 2005; Espinosa et al., 2006). Cantilever beams represent a very efficient solution in the field of MEMS applications (Ionescu, 2015; Zhang et al., 2014). The fundamental component of MEMS and NEMS cantilever devices is a suspended electrode above a fixed conductive substrate and actuated by a voltage difference, which exploits the switching of the flexible electrode between two stable positions (Loh and Espinosa, 2012; Chuang et al., 2010). A physical schematic of the MEMS cantilever beam is shown in Fig. 1a, where V_{out} and V_{PI} represent the input voltage applied to the micro-beams and the critical pull-in voltage of the system, respectively. Under the action of the electrostatic forces, the flexible micro-cantilever beam deflects towards the substrate (Fig. 1b) thus increasing the electrostatic force between the two electrodes. It comes that the flexible micro-cantilever becomes unstable, and then, at a critical voltage, named the pull-in voltage, the flexible electrode tip pulls-in onto the substrate (Fig. 1c), thus creating an electrical connection (Knapp and De Boer, 2002; Gorthi et al., 2006). This actuation scheme has been used in many

micro-nano scale devices, such as manipulators, tweezers, accelerometers, pressure sensors, memory devices and energy harvesting systems (Spaggiari et al., 2016). The purpose of these components is to process very fast communications (Eric Garfunkel, 2009) in addition to a smarter and very smaller micro-nano devices (Noghrehabadi et al., 2013). The planar technologies represent the most common actuation mechanism used in micro-nano MEMS devices giving their tiny size, low mass and high resonance frequency as well as the electrostatic actuation (Passian and Thundat, 2011). Since the critical pull-in voltage defines the operating voltage and power dissipation of the system, it must be accurately determined.

The first works on the nonlinear pull-in phenomenon are reported by Taylor (1968) and Wickstrom and Davis (1967) dating in the late 1960s. In the last years, Dequesnes et al. (2002) propose the use of parametrized continuum model that aims to calculate the pull-in voltages in nanoelectromechanical switches. The work of Ramezani et al. (2008a) focused on a general analytical method for the calculation of the pull-in instability in nano-cantilevers under electrostatic actuation. In particular, the work investigates a typical micro-nano actuator composed by a flexible beam and of a fixed plate with a very small gap separation between the two electrodes. The electromechanical behavior of the cantilever beams can be described by fourth-order nonlinear ordinary differential equation (ODE) and no exact solution can be obtained (Ramezani et al., 2008a). In this case, the modeling of the nonlinear response of the device must

* Corresponding author.

E-mail addresses: andrea.sorrentino@unimore.it (A. Sorrentino), giovanni.bianchi@unimore.it (G. Bianchi), enrico.radi@unimore.it (D. Castagnetti), davide.castagnetti@unimore.it (E. Radi).

<https://doi.org/10.1016/j.apples.2020.100014>

Received 6 September 2020; Accepted 10 September 2020

Available online xxx

2666-4968/© 2020 Published by Elsevier Ltd. This is an open access article under the CC BY license (<http://creativecommons.org/licenses/by/4.0/>)

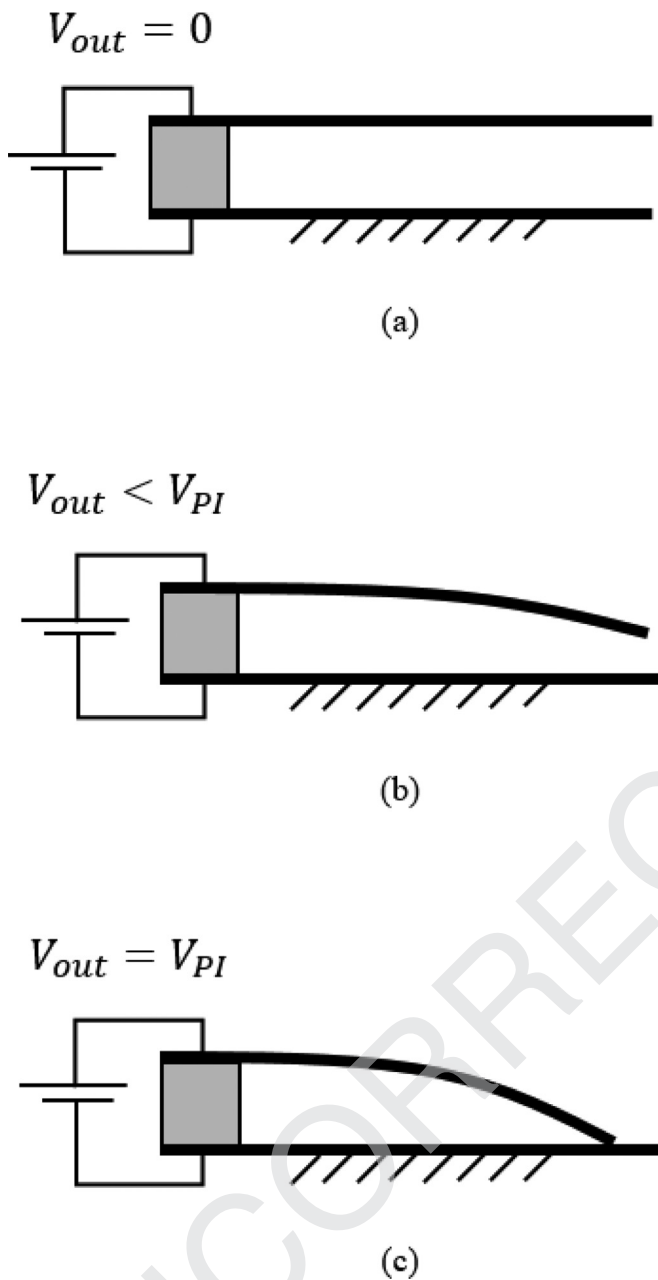


Fig. 1. The MEMS cantilever beam under different electrostatic voltage: no applied voltage (a), applied voltage lower than the critical pull-in limit (b), applied voltage at the pull-in (c).

48 take into account the dispersion forces of van der Waals (vdW) and
 49 Casimir (Ramezani et al., 2006; Soroush et al., 2010). Both the inter-
 50 molecular forces and the electrostatic actuation, influence the critical
 51 pull-in effects in MEMS-NEMS devices. Several numerical procedures
 52 and analytical methods can be traced in literature in order to estimate
 53 the pull-in parameters. The first approximated analytical approaches are
 54 the 1D based lumped model (Chowdhury et al., 2005), linearization
 55 methods (Noghrehabadi et al., 2012; Duan et al., 2013) or on Taylor
 56 series expansion of the loading term (Ghalambaz et al., 2011). In ad-
 57 dition, numerical or approximate techniques to generate reduced-order
 58 models are used; the most popular methods are the differential quadra-
 59 ture method, Adomian decomposition method, Galerkin method and fi-
 60 nite element method (Di Maida and Bianchi, 2016). On the other side,
 61 these approximated methods may provide large errors as the cantilever
 62 tip deflection increase closer to the pull-in stable position. Furthermore,

63 these approaches give non-specified estimates of the pull-in stability pa-
 64 rameters. By contrast, more accurate methods may provide the lower and
 65 upper bounds of the pull-in parameter, in order to ensure safely
 66 operating condition in the device. In particular, Radi et al. (2017), pro-
 67 pose an accurate analytical approach for estimating the lower and upper
 68 bounds to the critical pull-in characteristics for microcantilever actua-
 69 tors. The proposed model aims to predict the critical factors, geometri-
 70 cal and electromechanical, of electrostatically microcantilever actua-
 71 tors that lead the transition between two stable positions. In a second work,
 72 Radi et al. (2018) consider the effect of the compressive axial load on
 73 the pull-in voltage, to obtain an accurate estimate of the stable actuating
 74 range. A variety of recent works on the pull-in analysis and modeling
 75 are reported in literature (Fakhrabadi et al., 2013; Krylov, 2007; De and
 76 Aluru, 2004; Nayfeh et al., 2005; Chatterjee and Pohit, 2009; Zhao et al.,
 77 2004; Bochobza-Degani and Nemirovsky, 2004; Luo and Wang, 2002).
 78 In summary, a review describing the pull-in instability phenomenon,
 79 modeling and analysis for MEMS-NEMS devices is represented by the
 80 review report of Zhang et al. (2014). Generally, every electromechani-
 81 cal device can be affected by pull-in instability (Somà, 2007): some de-
 82 vices rely on the pull-in instability for the switching operation such as
 83 sensor and actuators, while in other devices such as micro-mirrors and
 84 radio frequency oscillators the pull-in instability is an undesired effect
 85 (Van Beek and Puers, 2012; Juillard, 2015). This supports the need for
 86 a simple and accurate model to predict the critical pull-in voltage. One
 87 of the main practical limitation comes from the pull-in voltage value: on
 88 the one hand, low pull-in voltage reduces the power consumption but
 89 increases the uncontrolled switching deflection thus causing failure. On
 90 the other hand, high pull-in voltage allows to avoid undesired failure
 91 but increase the power consumption, thus enhancing the device perfor-
 92 mance. The pull-in instability effects and the mechanical response of
 93 these actuators are defined by three main issues. First, the choice of the
 94 material of the MEMS-NEMS devices and the modeling of the boundary
 95 support for the elastic structures (Noghrehabadi et al., 2013; Rinaldi
 96 et al., 2005), both for the static and dynamic/vibrational electrostatic
 97 simulation of the deflected beam. Second, the presence of dispersion
 98 of the intermolecular surface forces. The interaction forces of van der
 99 Waals and Casimir depending on the gap separation between the two
 100 electrodes. As the gap decrease, namely below 20 nm for metals, the
 101 intermolecular forces becomes dominant, affecting the deflection and
 102 the stress-strain behavior of the nano-cantilever (Soroush et al., 2010;
 103 Ghalambaz et al., 2011). Third, the size dependency, also called size
 104 effect, that influences the mechanical properties of the cantilever when
 105 the size scale decrease rapidly (Stölken and Evans, 1998; Nix and Gao,
 106 1998). With regard to the experimental characterization of the pull-
 107 in instability in MEMS devices, a number of proposal can be found in
 108 literature in order to evaluate the nonlinear static behavior of micro-
 109 electrostatic actuators (Somà et al., 2019; Ballestra et al., 2008). First
 110 experimental validation and analysis on the pull-in instability have been
 111 performed by Taylor (1968), Wickstrom and Davis (1967) and Siddique
 112 et al. (2011). Poelma et al. (2011) evaluates the pull-in phenomenon for
 113 electrostatically paddle cantilever from 3D imaging reconstruction. Al-
 114 ternatively, Somà focused on detecting the mechanical fatigue limits in
 115 response to the pull-in voltage actuation in gold micro-beams specim-
 116 ens (Somà and De Pasquale, 2009; Soma et al., 2017), and experimentally
 117 validated the residual stress in electrostatically actuated radio frequency
 118 micromechanical systems (RF-MEMS), (De Pasquale and Soma, 2007;
 119 Somà and Saleem, 2015). The understanding and control of the pull-in
 120 instability represents, even now, a great technological challenge (Zhang
 121 et al., 2014). As a consequence of the high cost in the implementation of
 122 miniaturized specimens, combined with the need of specific instrumen-
 123 tation, is not simple to examine the robustness of the theoretical predic-
 124 tions for different type of actuator configurations. However, analytical
 125 approaches consider negligible Casimir and vdW surface forces, when
 126 the dimension of the cantilever beams shift to the micro scale, and con-
 127 sequently, in the millimeter scale. This work focuses on the experimen-
 128 tal characterization of the critical pull-in voltage and the tip deflection of a

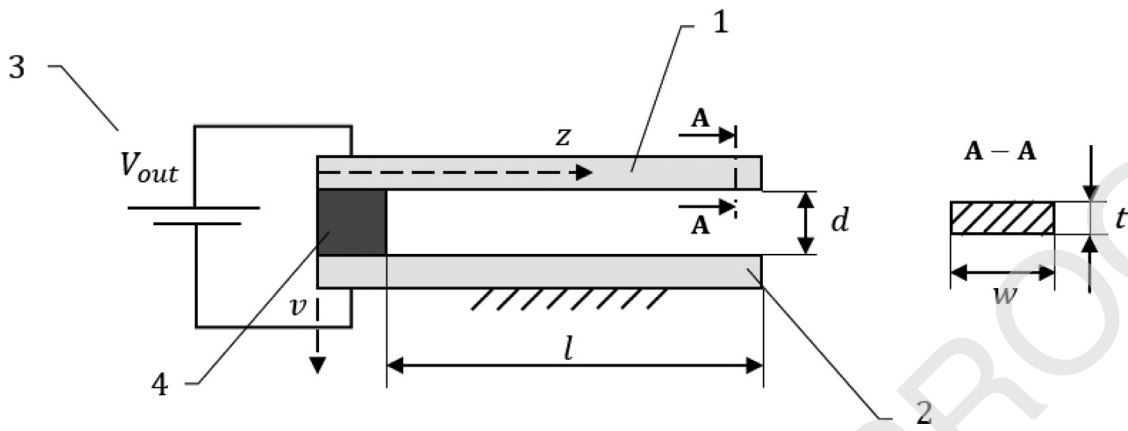


Fig. 2. The elastic micro-nano cantilever scheme subject to electrostatic actuation.

129 macro-scale size cantilever beam, with the aim to validate a theoretical
 130 micro-mechanical model proposed by Radi et al. (2017, 2018). Specific-
 131 ally, we designed and built a simple millimeter-scale cantilever, which
 132 was actuated through an ad-hoc electric circuit able to reproduce the
 133 same pull-in phenomenon observed in the micrometric scale. The tests
 134 investigated different cantilever configurations to examine the effect of
 135 the free length of the suspended electrode and the gap from the ground
 136 on the pull-in response. The proposed device is simply adaptable, low
 137 cost, and simple to manufacture. The experimental results exhibit a very
 138 good agreement with the analytical predictions (Radi et al., 2017, 2018).
 139 In particular, we obtained a relative difference between the experimen-
 140 tal and analytical values of the pull-in voltage in the range between from
 141 0.7% up to 10%, whereas the relative difference of the pull-in deflection
 142 falls in the range from 1.1% up to 18%.

143 2. Material and methods

144 Fig. 2 shows the configuration of the system examined in this work,
 145 which corresponds to the cantilever geometry and actuation scheme de-
 146 scribed in the works of Radi et al. (2017, 2018). Two plates compose
 147 the system: the flexible electrode (1), on top, and the ground (2), sub-
 148 ject to an electrostatic actuation (3), and separated by a dielectric layer
 149 (4). In order to evaluate the variation of the pull-in factor voltage with
 150 respect to the geometrical dimensions of the device, we examined differ-
 151 ent cantilever configurations. In particular, we tested different lengths
 152 of the beam in combination with different gaps of the dielectric layer.

153 2.1. The macro-scale model

154 Fig. 2 shows the generic elastic micro/nano cantilever of length, l ,
 155 width, w and thickness, t , clamped at one end, with $z = [0, l]$, and sub-
 156 ject to electrostatic actuation and intermolecular surface forces (Radi
 157 et al., 2017, 2018). In particular, we considered the non-dimensional
 158 deflection, $u = v/d$, and the axial coordinate, $x = z/l$, where v is the
 159 deflection, and d is the initial gap between the two electrodes, respec-
 160 tively. The system can be described mathematically by the following
 161 fourth-order nonlinear ordinary differential equation (ODE):

$$162 \quad u^{IV}(x) = \frac{\gamma\beta}{1-u(x)} + \frac{\beta}{[1-u(x)]^2} + \frac{\alpha_W}{[1-u(x)]^3} + \frac{\alpha_C}{[1-u(x)]^4} \quad (1.1)$$

$$163 \quad u(0) = u'(0) = 0, \quad u''(1) = u'''(1) = 0 \quad (1.2)$$

163 Where $\gamma = 0.65 d/w$ is the fringing coefficient. Moreover, the non-
 164 dimensional positive parameters β , α_W and α_C are proportional to the
 165 electrostatic, van der Waals and Casimir forces, respectively, namely:

$$\beta = \frac{\epsilon_0 w V^2 l^4}{2d^3 EI}$$

$$\alpha_W = \frac{A w l^4}{6\pi d^4 EI}$$

$$\alpha_C = \frac{\pi^2 h c w l^4}{240 d^5 EI} \quad (1.3)$$

Where $\epsilon_0 = 8.854 \cdot 10^{-12} \text{ C}^2 \text{ N}^{-1} \text{ m}^{-2}$ is the permittivity of vacuum, $h = 1.055 \cdot 10^{-34} \text{ Js}$ is the Planck's constant divided by 2π , $c = 2.998 \cdot 10^8 \text{ m/s}$ is the speed of light, A is the Hamaker constant, V is the electric voltage applied to the electrodes, E is the Young's modulus of the beam material and I is the moment of inertia of the beam cross-section. As show in Eq. (1.3), the parameters β , α_W and α_C affected considerably the values of the pull-in instability factors and then the operation point of the device. In particular, when the dimensions of the cantilever beams increase, the values of the intermolecular force parameters α_W and α_C decrease, consequently, if the dimensions of the actuator shift to the millimeter-scale the effect of the van der Waals and Casimir forces becomes negligible (α_W and α_C values fall in the range of $10^{-25} \div 10^{-28}$). In this operating condition, named the "macro-scale condition", only the electrostatic force determines the pull-in instability threshold of the beam. In addition, for an elastic material with a specific Young's modulus, E , the value of the parameter β allows to predict the value of the pull-in voltage with fixed geometrical parameters, w , t and l . By changing the geometric ratio, γ , the value of β changes and consequently the pull-in actuation voltage, see Eq. (1.1). In particular, the pull-in voltage for the macro-scale actuated cantilever beam, which depend on β , can be expressed by the following formula:

$$166 \quad V_{PI} = \sqrt{\beta \frac{2d^3 EI}{\epsilon_0 w l^4}} \quad (1.4)$$

167 Where, $I = \frac{w t^3}{12}$, is the moment of inertia for a rectangular cross-
 168 section area.

169 The macro-scale cantilever beam is able to reproduce the same
 170 electro-mechanical behavior observed in the micrometric scale (Radi
 171 et al., 2017, 2018). In the present investigation, we focused on the
 172 macro-scale model, where the intermolecular forces are negligible.
 173 While keeping constant the ratio between the geometrical dimensions
 174 of the system, it is possible to obtain a macro-scale model of the can-
 175 tilever by increasing the dimensions of the micro-system (Rollier et al.,
 176 2006). The corresponding critical pull-in deflection for the macro-scale
 177 model (Radi et al., 2017, 2018), named v_{PI} , fall in the range 44% ÷ 55%
 178 for a high fringing coefficient, specifically for $\gamma = 0 \div 3.25$, which corre-
 179 sponds to an air gap, d , five times greater than the width of the flex-
 180 ible beam, w (Sororoush et al., 2010; Ramezani et al., 2008b). To simplify
 181 the experimental approach, the authors suggest these following approxi-
 182 mated equations to compute the pull-in parameter considering the fring-
 183 ing field effect, β_{PI} for the pull-in voltage, and u_{PI} for the normalized
 184
 185
 186

204 pull-in deflection:

$$\beta_{PI} = \frac{1.67}{1 + 0.41\gamma}$$

$$u_{PI} = 0.6395 - \frac{2084}{10862 + 3069\gamma} \quad (1.5)$$

205 Using the analytical procedure described in Radi et al. (2017, 2018),
 206 lower and upper bounds are obtained for the pull-in parameters. Then,
 207 these estimates are used to fit the coefficients of the approximated re-
 208 lations (Eq. (1.5)) using the interpolation method available in Mathe-
 209 matica (Wolfram Research Inc 2020). The approximated curves fit very
 210 well with the lower and upper estimates of the pull-in voltage (Fig. 3a)
 211 and deflection (Fig. 3b) respectively, thus ensuring the accuracy of the
 212 approximated Eq. (1.5). Moreover, the approximated Eq. (1.5) for the
 213 voltage β_{PI} perfectly agrees with the approximated model introduced
 214 by Osterberg and Senturia (1997) and Ballestra et al. (2008).

215 2.2. Prototype development

216 First, the work focused on the design and prototype development of
 217 an adaptable millimeter-scale model of the MEMS device. The system
 218 is composed by two different parts: the mechanical one, formed by the
 219 switching system, the actuated cantilever, and the electrical part consist-
 220 ing of an electric circuit that regulates the input actuation on the device.
 221 In particular, the implemented device includes different pins output for
 222 the connection to the signal acquisition and monitoring system that reg-
 223 isters the electrostatically response of the system.

224 2.3. Actuated cantilever

225 The dimensions of the macro-scale model, and the related pull-in
 226 factors of the system, are affected by the geometric aspect ratios of the
 227 electrodes and by the value of the gap. From the work of Rollier et al.
 228 (2006), it is possible determine the cantilever's parameters relating to
 229 a system described by the Euler's theory, where, the geometric aspect
 230 ratios of the plates are represented by:

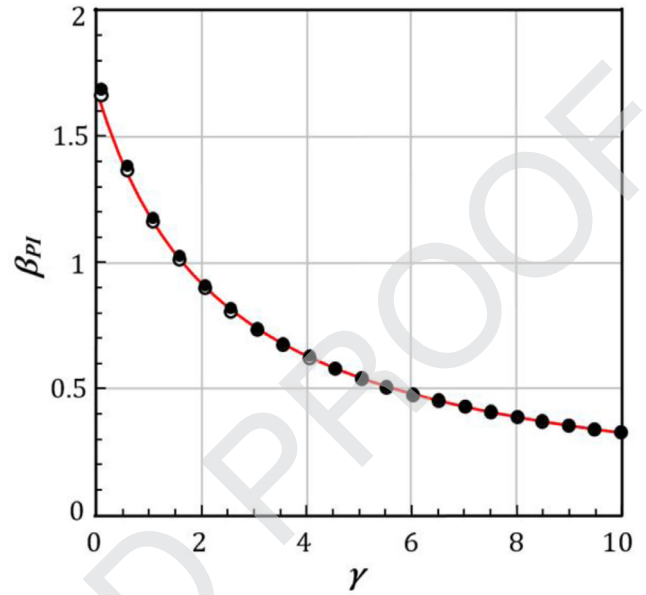
$$R_1 = \frac{w}{l}$$

$$R_2 = \frac{d}{l}$$

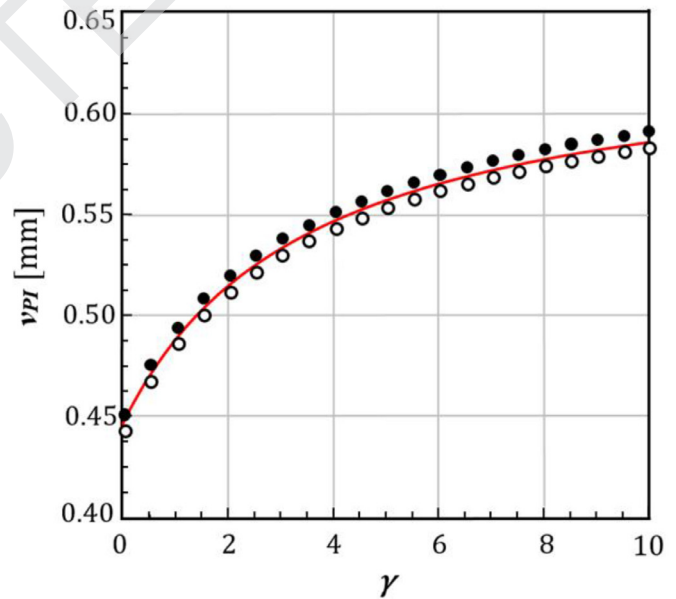
$$R_3 = \frac{t}{l}$$

$$R_4 = \frac{t}{w} \quad (2.1)$$

231 As show in the work of Somà (Ballestra et al., 2008), by keeping
 232 constant the ratio R_4 , the value of the pull-in voltage and deflection is
 233 affected by the values of the total free length of the flexible electrode,
 234 l , and from the gap, d . The increase in the scale, corresponds an in-
 235 crease of the voltage actuation for the cantilever beam. For this reason,
 236 a preliminary analysis of pull-in voltage and deflection was conducted
 237 with the aim to identify possible cantilever lengths, l , and predict the
 238 maximum pull-in voltage for different beam configurations (see Section
 239 "Test plan"). Hence, the maximum admissible pull-in voltage was set,
 240 for the macro-scale model, at 3000 V, for a gap, d , in the range be-
 241 tween 0.5 and 1 mm. Fig. 4 shows the case of planar plates with constant
 242 R_4 . The switching system is composed of two plates with a rectangu-
 243 lar cross-sectional area, the suspended and flexible electrode, and the
 244 fixed ground, both made of steel C100S with nominal Young's modulus,
 245 $E = 210,000 \text{ MPa}$, and a Poisson's ratio, ν , equal to 0.3. The electrodes
 246 of the system are simply obtained from a commercial steel tape, with the
 247 aim to have planar and lightweight beams. The plates of the system have
 248 a thickness, $t = 0.2 \text{ mm}$, and a width, $w = 12.7 \text{ mm}$, which correspond
 249 to an $R_4 = 0.0157$. The free length, l , of the suspended electrode was
 250 set initially equal to 50 mm, while the gap between the two electrodes
 251 was set equal to 0.6 mm and obtained through a simple bi-adhesive tape
 252 (Fig. 4), which makes easier the assembly of the flexible electrode on the



(a)



(b)

Fig. 3. The normalized pull-in voltage, β_{PI} , with respect to the variation of the fringing coefficient, γ (a), the normalized deflection u_{PI} with respect to γ (b). The continues curves represents the approximated solution, and the black dot and the empty circle the analytic estimate for the upper and lower bounds, respectively.

253 dielectric support. The flexible electrode was placed on the bi-adhesive 253
 254 tape by pliers and then, the gap height d , was measured by an altimeter. 254
 255 From the analytical model of Radi et al. (2017, 2018), it is possible to 255
 256 calculate the pull-in parameter β of the system (see Eqs. (1.1) and (1.5)) 256
 257 for fixed w , t , l and d and the corresponding analytical pull-in voltage, 257
 258 V_{PI} (see Eq. (1.4)). 258

259 2.4. Power circuit

260 Due to the macro scale, the device requires a high actuation volt- 260
 261 age to reach the pull-in. For this reason, we used a high voltage DC-DC 261

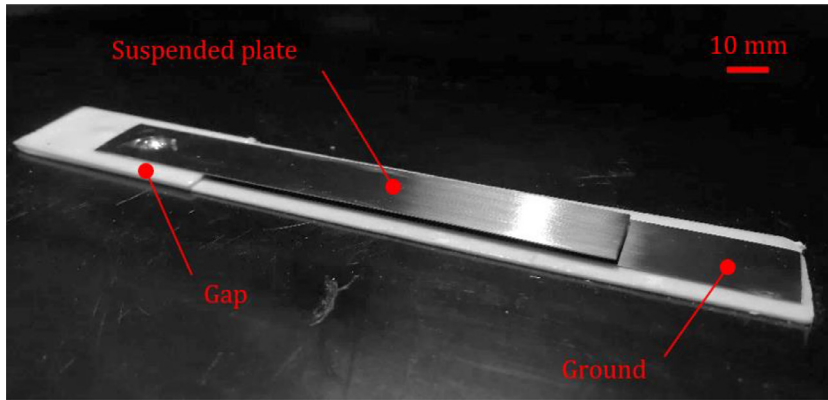


Fig. 4. Millimeter scale device implemented.

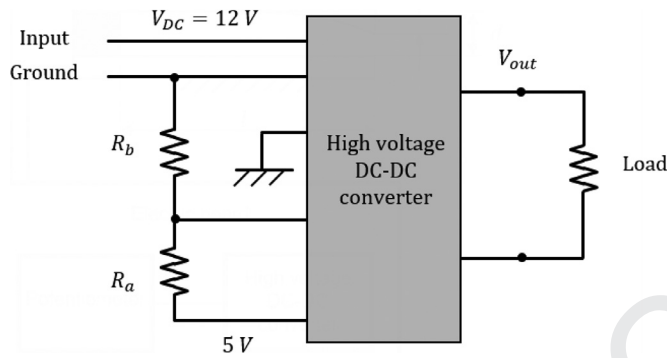


Fig. 5. The operating circuit of the converter.

262 converter (EMCO CB101) powered at 12 V through a power supply and
 263 giving an output voltage, V_{out} , in a range between 0 and ± 10 kV. Fig. 5
 264 shows the operating circuit of the device.

265 Specifically, we have the high voltage DC-DC converter, and a simple
 266 circuit that allows to regulate the output voltage, V_{out} , which is the
 267 actuation voltage for the flexible cantilever. The regulation circuit consists
 268 of a voltage divider with electric resistances, R_a and R_b . Based on
 269 the schematic in Fig. 5, the output voltage of the device, V_{out} , is related
 270 to the value of the resistances R_a and R_b (Fig. 5) through the following
 271 equation:

$$V_{out} = \frac{R_a}{R_a + R_b} * (10,000) \quad (2.2)$$

272 By keeping a high value for R_b , about 10 k Ω , the corresponding V_{out}
 273 of the converter is provided by the value of R_a . By replacing the two
 274 resistors R_a and R_b with a manual multi-turn potentiometer, we can
 275 regulate the output voltage from the DC-DC converter, from 0 up to
 276 the pull-in threshold, V_{PI} , thus, the corresponding output voltage, V_{out} ,
 277 can be computed by Eq. (2.2). The critical value of the output voltage
 278 corresponds to the pull-in voltage, V_{PI} , as mentioned in Section 1. The
 279 high voltage output pin of the converter is finally connected on the top
 280 surface of the suspended electrode where the macro-beam is bonded.
 281 Fig. 6 shows the implemented electric circuit solution that includes all
 282 the electrical components of the power circuit, that are the DC-DC
 283 converter and the potentiometer. It is remarkable that the value of the current
 284 trough the circuit is maintained very low, about 200 mA, far below
 285 the possible critical value for failure. When pull-in occurs, the high voltage
 286 converter turns off, avoiding high electric charge on the circuit.

287 2.5. Experimental set-up

288 The experimental validation aims to measure the critical pull-in voltage
 289 and deflection of the cantilever beam. Fig. 7 shows the schematic of
 290 the test bench for the experimental validation.

291 In order to measure the tip deflection of the suspended electrode,
 292 we used a single point laser-doppler vibrometer (Polytec OFV-505 sensor
 293 head) with a tolerance on the position of 0.002 mm. The vibrometer
 294 points to the tip of the flexible electrode, in the vertical direction
 295 with respect to the initial top surface of the flexible electrode (Immovilli
 296 et al., 2013, 2011), Fig. 7. The vibrometer is managed by a National
 297 Instrument data acquisition board (NI 9211). The acquisition board also
 298 measure the pull-in voltage connected to the device. Before applying
 299 the actuation voltage to the device, we ensured that the beams were
 300 discharged, in order to avoid early pull-in phenomenon due to residual
 301 electrical charge in the electrodes. When the power circuit is on, the
 302 flexible micro-cantilever beam deflects towards to the substrate under the
 303 action of the electrostatic forces provided by the high voltage converter,
 304 and the vibrometer simultaneously and continuously recorded the
 305 corresponding tip deflection, until the system reached the pull-in. The slow
 306 regulation of the input voltage thanks to the potentiometer, prevented
 307 voltage fluctuation during the actuation of the system and thus made
 308 possible to acquire the effective pull-in voltage of the beam. The acquisition
 309 board was connected to a pc that registered and processed the data
 310 using an algorithm implemented in the LabVIEW environment (Bitter
 311 et al., 2020).

312 2.6. Test plan

313 In order to assess the accuracy of the prototype, we tested some dif-
 314 ferent configurations of the cantilever to examine the influence of some
 315 parameters on the pull-in. For this investigations we considered constant
 316 nominal width, $w = 12.7$ mm, as reported in the work of Ballestra et al.
 317 (2008), and nominal thickness, $t = 0.2$ mm, for all the specimens tested
 318 (see Section "Actuated cantilever"). Specifically, we investigated three
 319 levels of free length, l , in combination with two different gaps from the
 320 ground, d . Table 1 reports the six cantilever configurations investigated
 321 experimentally. For all the six configurations in Table 1, we performed
 322 ten replications of the pull-in tests, for a total of 60 tests. Each of the six
 323 configurations tested was manufactured as a completely new specimen.

324 3. Results

325 Table 2 compares the critical pull-in parameters for the six config-
 326 urations investigated (see Table 1) where, V_{PI}^E and V_{PI}^A , represent the
 327 experimental and the analytical pull-in voltages, respectively, and v_{PI}^E
 328 and v_{PI}^A the corresponding pull-in deflections, using the analytical model
 329 provided by Radi et al. (2017, 2018).

330 In particular, for the experimental pull-in voltage and deflection, we
 331 reported the mean value and the corresponding standard deviation for
 332 the 10 replications performed. Figs. 8 and 9 show, respectively, the rela-
 333 tion between the experimental pull-in voltage, V_{PI}^E , and the deflection,
 334 v_{PI}^E , with respect to the variation of the gap, d , and of the total free
 335 length, l .

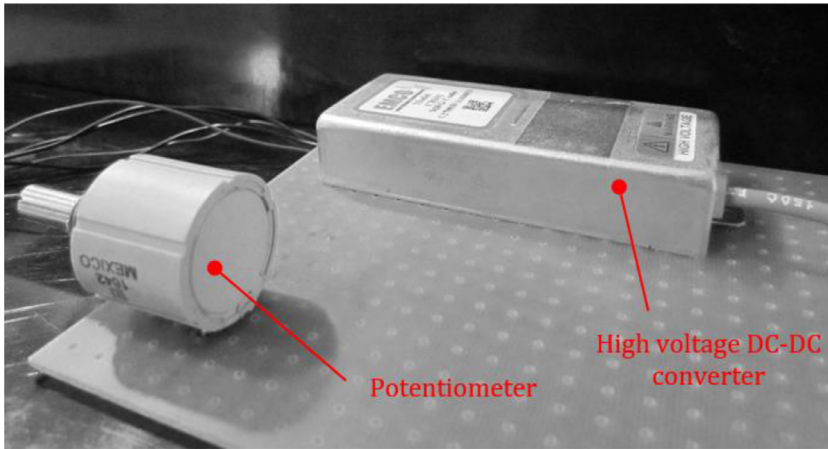


Fig. 6. The electric board and the converter circuit implemented.

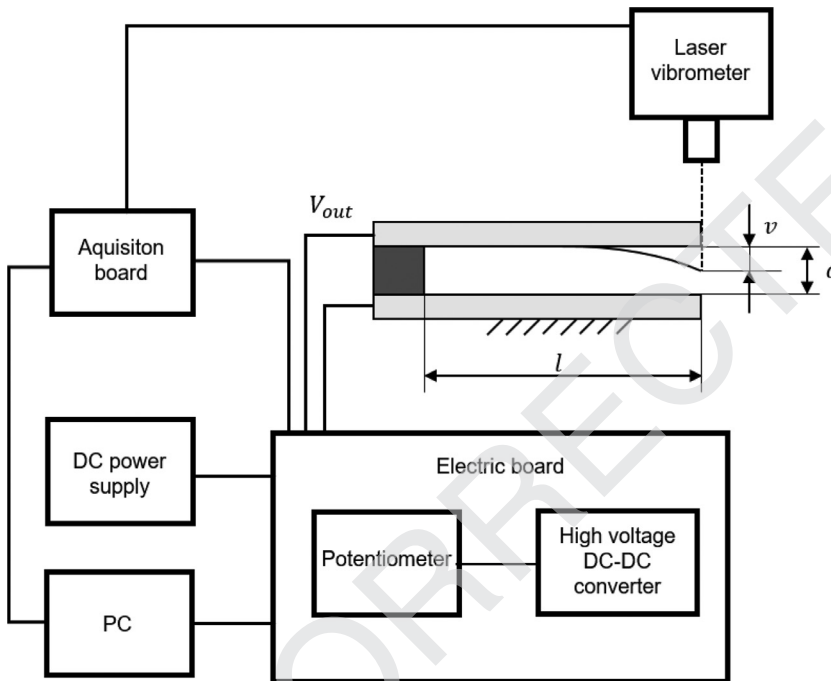


Fig. 7. Schematic of the testing benchmark.

Table 1
Nominal dimensions and related aspect ratios for the different specimens tested.

Specimen	l [mm]	w [mm]	t [mm]	d [mm]	R_1	R_2	R_3	R_4
1	50.00±0.02	12.7	0.2	0.60±0.02	0.254	0.012	0.004	0.016
2	60.00±0.02	12.7	0.2	0.60±0.02	0.212	0.01	0.003	0.016
3	70.00±0.02	12.7	0.2	0.60±0.02	0.181	0.009	0.003	0.016
4	50.00±0.02	12.7	0.2	0.80±0.02	0.254	0.016	0.004	0.016
5	60.00±0.02	12.7	0.2	0.80±0.02	0.212	0.013	0.003	0.016
6	70.00±0.02	12.7	0.2	0.80±0.02	0.181	0.011	0.003	0.016

336 The critical pull-in values obtained experimentally and analytically
 337 are compared to the value of the critical pull-in factors obtained numerically
 338 numerically by the shooting method (Osborne, 1969) implemented in the
 339 Mathematica software Mathematica (Wolfram Research Inc 2020). The
 340 diagrams in Figs. 10 and 11 relate the pull-in voltage, y axis of the graph,
 341 and the pull-in deflection, x axis of the graph, for the two different gaps
 342 considered.

343 4. Discussion

344 As shown in Figs. 8 and 9 it appears that both the variable free length,
 345 l , and the value of the gap, d , of the device affected the amount of the

pull-in voltage significantly: on the one hand, the higher the length of
 346 the flexible electrode, l , the higher the value of the pull-in voltage. On
 347 the other hand, by decreasing the value of the gap, d , the pull-in voltage
 348 decreases according to the analytical prediction model (Radi et al., 2017,
 349 2018). The experimental results in Table 2 exhibit a very good agree-
 350 ment with the analytical predictions from the model proposed by Radi
 351 et al. (2017, 2018). In particular, the relative difference between the
 352 experimental measurements and analytical values of the pull-in voltage
 353 falls in the range between 0.7% and 10%, whereas the relative differ-
 354 ence for the pull-in deflection falls in the range from 1.1% up to 18%
 355 (Table 2). In addition, Figs. 10 and 11 highlight that the pull-in critical
 356 values provided by the shooting method (Osborne, 1969) closely match
 357

Table 2

Comparison between the experimental and analytical pull-in voltage and tip deflection.

Specimen	V_{PI}^E [V]	V_{PI}^A [V]	v_{PI}^E [mm]	v_{PI}^A [mm]
1	1261 ± 19	1337	0.262 ± 0.024	0.268
2	891 ± 42	929	0.263 ± 0.018	0.268
3	682 ± 25	682	0.273 ± 0.018	0.268
4	2047 ± 28	2052	0.298 ± 0.050	0.357
5	1423 ± 16	1425	0.359 ± 0.028	0.357
6	942 ± 93	1047	0.391 ± 0.016	0.357

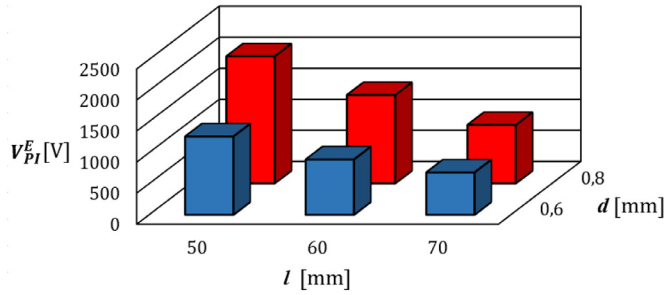


Fig. 8. The experimental pull-in voltage variation for the different cases evaluated.

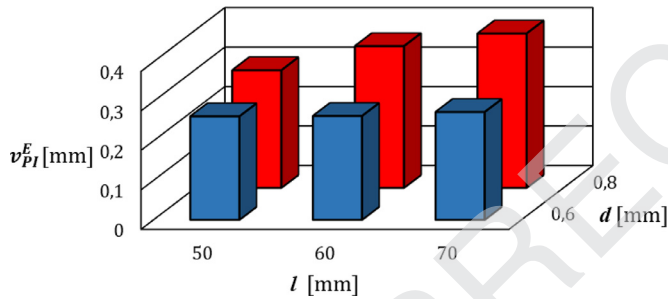


Fig. 9. The experimental pull-in deflections measured.

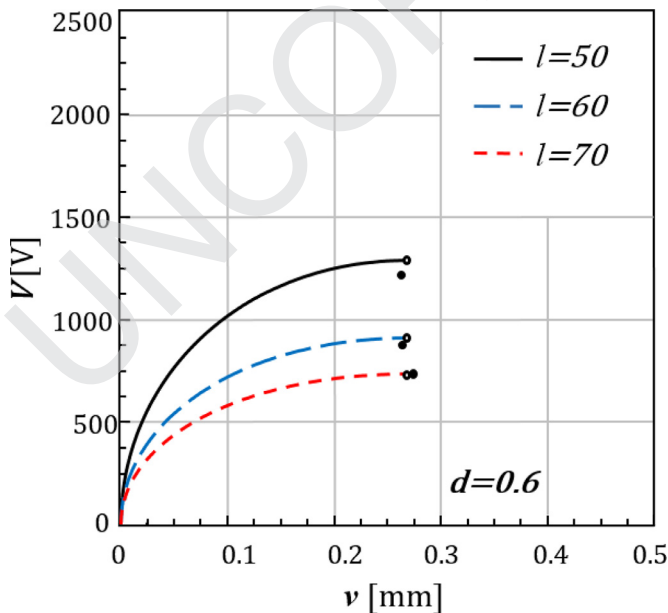


Fig. 10. The pull-in voltage, V_{PI} , with respect to the deflection, v , for different free lengths, l , and for a fixed gap, g , equal to 0.6 mm. The solid lines represent the numerical solution, the black dots the experimental estimates, and the white circles the analytical estimates, respectively.

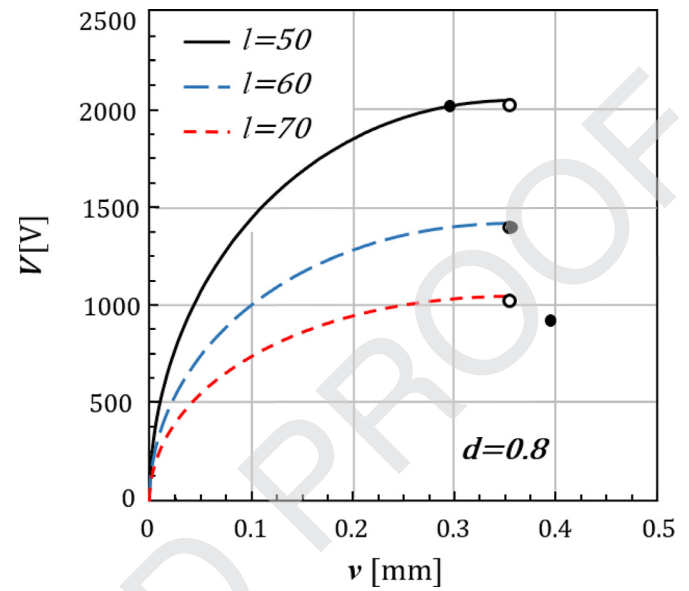


Fig. 11. The pull-in voltage, V_{PI} , with respect to the variation of the deflection, v , for different free length, l , and for fixed gap, g , equal to 0.8 mm. The solid lines represent the numerical solution, the black dots the experimental estimates, and the white circles the analytical estimates, respectively.

the experimental measurements. From Table 2, we can observe a significant scatter in the values of the pull-in voltage and deflection, that can be imputed to the following geometrical issues. First, the combined effect of the inaccuracies in the air gap, d , and in the free length, l , of the experimental device: for instance, according to the analytical model (Eq. (1.4) and 1.5), a 0.01 mm variation in the gap, d , combined with a 0.1 mm variation of the free length, l , give a scatter of the pull-in voltage from about 20 up to 47 V. Second, small inaccuracies in the positioning of the mobile plate on the bi-adhesive gap gives not perfect alignment on the clamped cantilever thus affecting the planarity between the two electrodes. Third, the higher the free length, l , the higher the effect of the weight of the flexible plate, see Table 2. Nevertheless, the proposed analytical model by Radi et al. (2017, 2018), gives an accurate prediction of the experimental behavior of the system, also compared to previous works in the literature (Ballestra et al., 2008) and Rollier et al., 2006). The proposed macro-scale model is a low-cost solution with the only limitation of a high actuation voltage to reach the pull-in threshold (Table 2). With regard to prototype manufacturing, the proposed solution has the following advantages. First, the macro scale prototype is more simple and quick to set-up, compared to a micro-nano scale solution. Second, by changing the cantilever configuration, it is possible to test different macro-scale models, thanks to the fact that the electric board of the prototype is external and isolated from the switching part. Third, the macro-scale prototype implemented allows to recreate the same switching phenomenon observed in the nano scale, with exception of the Casimir and vdW surface forces. In addition, considering the fringing effect in the analytical model also for the macro-scale solution (Eqs. (1.4) and (1.5)), the experimental results show a remarkable improvement compared to the models in the literature, see Figs. 10 and 11.

5. Conclusions

The present work assesses a previous analytical model from the literature via experimental tests with the use of a simple millimeter-scale device, which was actuated through an ad-hoc electric circuit. The work aimed to measure the critical pull-in voltage and the deflection of an actuated cantilever beam for different configurations in order to validate the variation of the pull-in voltage with the geometrical parameters

of the device provided by theoretical investigations. Analytical predictions closely match the experimental estimates, where the maximum relative difference between experimental and analytical values of the pull-in voltage is in the order of 10%, whereas the relative difference of the pull-in deflection falls below 18%. The adaptable prototype developed allowed to evaluate different cantilever configurations, then, the influence of the geometrical and electromechanical parameters for the system on the pull-in instability. The proposed macro-scale prototype is a very quick and smart solution from a manufacturing standpoint.

404 Funding

405 This research did not receive any specific grant from funding agencies in the public, commercial, or not-for-profit sectors.

407 Uncited reference

408 (Cheng et al., 2004).

409 Declaration of Competing Interest

410 All authors agree on the submission of the paper in the present form.

411 References

- 412 Ballestra, A., Brusa, E., Munteanu, M.G., et al., 2008. Experimental characterization of
413 electrostatically actuated in-plane bending of microcantilevers. *Microsyst. Technol.*
414 14, 909–918.
- 415 Bitter R., Mohiuddin T., Nawrocki M. 2020 Labview: Advanced Programming Techniques.
416 Bochobza-Degani, O., Nemirovsky, Y., 2004. Experimental verification of a design method-
417 ology for torsion actuators based on a rapid pull-in solver. *J. Microelectromech. Syst.*
418 13, 121–130.
- 419 Chatterjee, S., Pohit, G., 2009. A large deflection model for the pull-in analysis of electro-
420 statically actuated microcantilever beams. *J. Sound Vib.* 322, 969–986.
- 421 Cheng, J., Zhe, J., Wu, X., 2004. Analytical and finite element model pull-in study of rigid
422 and deformable electrostatic microactuators. *J. Micromech. Microeng.* 14, 57–68.
- 423 Chowdhury, S., Ahmadi, M., Miller, W.C., 2005. A closed-form model for the pull-in volt-
424 age of electrostatically actuated cantilever beams. *J. Micromech. Microeng.* 15, 756–
425 763.
- 426 Chuang, W.C., Lee, H.L., Chang, P.Z., et al., 2010. Review on the modeling of electrostatic
427 MEMS. *Sensors* 10, 6149–6171.
- 428 De, S.K., Aluru, N.R., 2004. Full-Lagrangian schemes for dynamic analysis of electrostatic
429 MEMS. *J. Microelectromech. Syst.* 13, 737–758.
- 430 De Pasquale, G., Soma, A., 2007. Design and finite element simulation of MEMS for fatigue
431 test. In: *Proceedings of the International Semiconductor Conference*, 1. CAS, pp. 159–
432 162.
- 433 Dequesnes, M., Rotkin, S.V., Aluru, N.R., 2002. Calculation of pull-in voltages for carbon-
434 nanotube-based nanoelectromechanical switches. *Nanotechnology* 13, 120–131.
- 435 Di Maida, P., Bianchi, G., 2016. Numerical investigation of pull-in instability in a
436 micro-switch MEMS device through the pseudo-spectral method. *Model. Simul. Eng.*
437 doi:10.1155/2016/8543616, Epub ahead of print 2016.
- 438 Duan, J.S., Rach, R., Wazwaz, A.M., 2013. Solution of the model of beam-type micro- and
439 nano-scale electrostatic actuators by a new modified Adomian decomposition method
440 for nonlinear boundary value problems. *Int. J. Non Linear Mech.* 49, 159–169.
- 441 Eric Garfunkel A.D. *Advanced Materials and Technologies for Micro / Nano-Devices, Sensors*
442 *and Actuators NATO Science for Peace and Security Series*. 2009.
- 443 Espinosa H.D., Ke C., Pugno N. *Nanoelectromechanical Systems: Experiments and Modeling*.
444 2006. Epub ahead of print 2006. doi:10.1016/b0-08-043152-6/02134-3.
- 445 Fakhrabadi, M.M.S., Khorasani, P.K., Rastgoo, A., et al., 2013. Molecular dynamics sim-
446 ulation of pull-in phenomena in carbon nanotubes with Stone-Wales defects. *Solid*
447 *State Commun.* 157, 38–44.
- 448 Ghalambaz, M., Noghrehabadi, A., Abadyan, M., et al., 2011. A new power series solu-
449 tion on the electrostatic pull-in instability of nano cantilever actuators. *Proc. Eng.* 10,
450 3708–3716.
- 451 Gorthi, S., Mohanty, A., Chatterjee, A., 2006. Cantilever beam electrostatic MEMS actu-
452 ators beyond pull-in. *J. Micromech. Microeng.* 16, 1800–1810.
- 453 Immovilli, F., Bianchini, C., Cocconcelli, M., et al., 2011. Currents and vibrations in asyn-
454 chronous motor with externally induced vibration. In: *Proceedings of the SDEMPED*
455 *2011 - 8th IEEE Symposium on Diagnostics for Electrical Machines, Power Electronics*
456 *and Drives*, pp. 580–584.
- 457 Immovilli, F., Bianchini, C., Cocconcelli, M., et al., 2013. Bearing fault model for induction
458 motor with externally induced vibration. *IEEE Trans. Ind. Electron.* 60, 3408–3418.
- 459 Ionescu, A.M., 2015. Nano-Electro-Mechanical (NEM) memory devices. *Emerg. Nanoelec-*
460 *tron. Devices* 9781118447, 123–136.
- 461 Juillard, J., 2015. Analysis of resonant pull-in of micro-electromechanical oscillators. *J.*
462 *Sound Vib.* 350, 123–139.
- 463 Ke, C.H., Pugno, N., Peng, B., et al., 2005. Experiments and modeling of carbon nanotube-
464 based NEMS devices. *J. Mech. Phys. Solids* 53, 1314–1333.

- Knapp, J.A., De Boer, M.P., 2002. Mechanics of microcantilever beams subject to combined
465 electrostatic and adhesive forces. *J. Microelectromech. Syst.* 11, 754–764.
- 466 Krylov, S., 2007. Lyapunov exponents as a criterion for the dynamic pull-in instability of
467 electrostatically actuated microstructures. *Int. J. Non Linear Mech.* 42, 626–642.
- 468 Loh, O.Y., Espinosa, H.D., 2012. Nanoelectromechanical contact switches. *Nat. Nanotech-*
469 *no.* 7, 283–295.
- 470 Luo, A.C.J., Wang, F.Y., 2002. Chaotic motion in a micro-electro-mechanical system with
471 non-linearity from capacitors. *Commun. Nonlinear Sci. Numer. Simul.* 7, 31–49.
- 472 Nayfeh, A.H., Younis, M.I., Abdel-Rahman, E.M., 2005. Reduced-order models for MEMS
473 applications. *Nonlinear Dyn.* 41, 211–236.
- 474 Nix, W.D., Gao, H., 1998. Indentation size effects in crystalline materials: a law for strain
475 gradient plasticity. *J. Mech. Phys. Solids* 46, 411–425.
- 476 Noghrehabadi, A., Ghalambaz, M., Ghanbarzadeh, A., 2012. A new approach to the elec-
477 trostatic pull-in instability of nanocantilever actuators using the ADM-Padé technique.
478 *Comput. Math. Appl.* 64, 2806–2815.
- 479 Noghrehabadi, A., Eslami, M., Ghalambaz, M., 2013. Influence of size effect and elastic
480 boundary condition on the pull-in instability of nano-scale cantilever beams immersed
481 in liquid electrolytes. *Int. J. Non Linear Mech.* 52, 73–84.
- 482 Osborne, M.R., 1969. On shooting methods for boundary value problems. *J. Math. Anal.*
483 *Appl.* 27, 417–433.
- 484 Osterberg, P.M., Senturia, S.D., 1997. M-test: a test chip for MEMS material property mea-
485 surement using electrostatically actuated test structures. *J. Microelectromech. Syst.* 6,
486 107–118.
- 487 Passian, A., Thundat, T., 2011. Chapter 2262 - microcantilever sensors. *Encycl. Mater. Sci.*
488 *Technol.* 1–6.
- 489 Poelma, R.H., Sadeghian, H., Noijen, S.P.M., et al., 2011. A numerical experimental ap-
490 proach for characterizing the elastic properties of thin films: application of nanocan-
491 tilevers. *J. Micromech. Microeng.* 21. doi:10.1088/0960-1317/21/6/065003, Epub
492 ahead of print.
- 493 Radi, E., Bianchi, G., di Ruvo, L., 2017. Upper and lower bounds for the pull-in parameters
494 of a micro- or nanocantilever on a flexible support. *Int. J. Non Linear Mech.* 92, 176–
495 186.
- 496 Radi, E., Bianchi, G., di Ruvo, L., 2018. Analytical bounds for the electromechanical buck-
497 ling of a compressed nanocantilever. *Appl. Math. Model.* 59, 571–582.
- 498 Ramezani, A., Alasty, A., Akbari, J., 2006. Influence of van der Waals force on the pull-in
499 parameters of cantilever type nanoscale electrostatic actuators. *Microsyst. Technol.*
500 12, 1153–1161.
- 501 Ramezani, A., Alasty, A., Akbari, J., 2008. Closed-form solutions of the pull-in instability
502 in nano-cantilevers under electrostatic and intermolecular surface forces. *Int. J. Solids*
503 *Struct.* 45, 2598–2612.
- 504 Ramezani, A., Alasty, A., Akbari, J., 2008. Closed-form solutions of the pull-in instability
505 in nano-cantilevers under electrostatic and intermolecular surface forces. *Int. J. Solids*
506 *Struct.* 45, 2598–2612.
- 507 Rinaldi, G., Packirisamy, M., Stiharu, I., 2005. Multi-parameter synthesis of microsystems.
508 *Photonics Appl. Devices Commun. Syst.* 5970, 597016.
- 509 Rollier, A.S., Legrand, B., Collard, D., et al., 2006. The stability and pull-in voltage of
510 electrostatic parallel-plate actuators in liquid solutions. *J. Micromech. Microeng.* 16,
511 794–801.
- 512 Siddique, J.I., Deaton, R., Sabo, E., et al., 2011. An experimental investigation of the
513 theory of electrostatic deflections. *J. Electrostat.* 69, 1–6.
- 514 Somà, A., De Pasquale, G., 2009. MEMS mechanical fatigue: experimental results on gold
515 microbeams. *J. Microelectromech. Syst.* 18, 828–835.
- 516 Somà, A., Saleem, M.M., 2015. Modeling and experimental verification of thermally in-
517 duced residual stress in RF-MEMS. *J. Micromech. Microeng.* 25, 55007.
- 518 Somà, A., Saleem, M.M., Margesin, B., et al., 2019. Pull-in tests of MEMS specimens for
519 characterization of elastic-plastic behavior. *Microsyst. Technol.* 4396.
- 520 Somà, A., 2007. MEMS Design for reliability: mechanical failure modes and testing. *Pers-*
521 *pect. Technol. Methods MEMS Des.* 0, 296.
- 522 Soma, A., Saleem, M.M., Margesin, B., 2017. Experimental characterization of elastic-
523 plastic behavior of MEMS electroplated gold specimens. In: *Proceedings of the Sym-*
524 *posium on Design, Test, Integration and Packaging of MEMS/MOEMS, DTIP, 2017*
525 doi:10.1109/DTIP.2017.7984501, Epub ahead of print.
- 526 Soroush, R., Koochi, A., Kazemi, A.S., et al., 2010. Investigating the effect of Casimir and
527 van der Waals attractions on the electrostatic pull-in instability of nano-actuators.
528 *Phys. Scr.* 82. doi:10.1088/0031-8949/82/04/045801, Epub ahead of print.
- 529 Spaggiari A., Castagnetti D., Golinelli N., et al. *Smart Materials: Properties, Design and*
530 *Mechatronic Applications*. 2016; 0: 1–29.
- 531 Stölken, J.S., Evans, A.G., 1998. A microbend test method for measuring the plasticity
532 length scale. *Acta Mater.* 46, 5109–5115.
- 533 Taylor, G., 1968. A PRSL. The coalescence of closely spaced drops when they are at dif-
534 ferent electric potentials. In: *Proceedings of the Royal Society of London Series A*
535 *Mathematical and Physical Sciences*, 306, pp. 423–434.
- 536 Van Beek, J.T.M., Puers, R., 2012. A review of MEMS oscillators for fre-
537 quency reference and timing applications. *J. Micromech. Microeng.* 22,
538 doi:10.1088/0960-1317/22/1/013001, Epub ahead of print.
- 539 Wickstrom, R.a., Davis, J.R., 1967. Gate transistor. *IEEE Trans. Electron Devices* 14, 117–
540 133.
- 541 Wolfram Research Inc. 2020 *Mathematica* 9.0.
- 542 Zhang, W.M., Yan, H., Peng, Z.K., et al., 2014. Electrostatic pull-in instability in
543 MEMS/NEMS: a review. *Sens. Actuators A* 214, 187–218.
- 544 Zhao, X., Abdel-Rahman, E.M., Nayfeh, A.H., 2004. A reduced-order model for electrically
545 actuated microplates. *J. Micromech. Microeng.* 14, 900–906.
- 546